 CMES, vol.62, no.2, pp.205-222, 2010

A Finite Element enrichment technique by the Meshless Local Petrov-Galerkin method

M. Ferronato[1], **A. Mazzia**[1] **and G. Pini**[1]

Abstract: In the engineering practice meshing and re-meshing complex domains by Finite Elements (FE) is one of the most time-consuming efforts. Meshless methods avoid this task but are computationally more expensive than standard FE. A somewhat natural improvement can be attempted by combining the two techniques with the aim at emphasizing the respective merits. The present work describes a FE enrichment by the Meshless Local Petrov-Galerkin (MLPG) method. The basic idea is to add a limited number of moving MLPG points over a fixed coarse FE grid, in order to improve the solution accuracy in specific regions of the domain with no mesh refinements. The transient Poisson equation is used as a test problem, with the numerical convergence of the enriched FE-MLPG method verified in several cases. The enriched approach proves more accurate than standard FE even by a factor 15 with a small number of MLPG nodes added.

Keywords: Finite Element, Meshless Local Petrov-Galerkin, enrichment, convergence analysis.

1 Introduction

The broadening of computer simulations in different engineering fields has progressively revealed the limitations of most traditional and conventional numerical meshbased techniques, such as Finite Elements (FE), Finite Volumes (FV) or Finite Differences (FD). A major drawback of such methods stems from the need for a conforming grid of the domain of interest satisfying some regularity constraints which often cannot be easily met. These limitations can be overcome by the use of meshfree methods that aim at eliminating the mesh dependency building an approximate solution in terms of nodes only. For instance, meshfree methods are particularly effective wherever large deformations occur, e.g. in manifacturing processes [Wang, Chen and Sun (2003); Ching and Chen (2006)], high-

[1] Dept. Mathematical Methods and Models for Scientific Applications (DMMMSA) – University of Padova, via Trieste 63, 35121 Padova, Italy.

speed impact and penetration analyses [Han, Rajendran and Atluri (2005); Han, Liu, Rajendran and Atluri (2006)], geomechanics of soft and loose soils [Deeks and Augarde (2007); Heaney, Augarde and Deeks (2010)]. Despite some recent developments [Wells, Borst and Sluys (2002); Liu and Borja (2008)], the implementation of fractures and discontinuities not coinciding with elemental edges is much simpler using meshfree techniques, e.g. [Gao, Liu and Liu (2006); Sladek, Sladek, Zhang, Solek and Starek (2007)]. Dynamic processes, such as explosions, the evolution of dust clouds and the micro-mechanics of granular materials, are successfully simulated using particle methods, e.g. [Randles and Libersky (2000); Fernandez-Mendez, Bonet and Huerta (2005)], as well as problems with singular or almost-singular solutions, e.g. [Wang, Chen and Sun (2003); Johnson and Owen (2007)]. Other recent applications of meshfree methods are in the fields of poro-elasticity [Ferronato, Mazzia, Pini and Gambolati (2007); Bergamaschi, Martinez and Pini (2009)], thermo-elasticity [Sladek, Sladek, Zhang and Tan (2006)], heat conduction [Wu, Shen and Tao (2007)], and non-steady fluid flow around moving surfaces [Avila and Atluri (2010)].

Meshfree methods can be basically grouped into three classes: 1) collocation techniques, e.g. Smooth Particle Hydrodynamic (SPH, [Randles and Libersky (1996)]); 2) Galerkin variational methods, e.g. Element-Free Galerkin (EFG, [Belytschko, Lu and Gu (1994)]) and Reproducing Kernel Particle Method (RKPM, [Liu, Jun and Zhang (1995)]); and 3) Petrov-Galerkin variational methods, e.g. Meshless Local Petrov-Galerkin (MLPG, [Atluri and Zhu (1998)]). While collocation techniques seek the solution as a convolution integral of window functions, variational methods such as EFG or MLPG are generally based on the Moving Least Square (MLS) approximation scheme. Amongst the methods above, MLPG appears to be one of the most promising as it is a "truly" meshless approach which does not require any connection between the nodes not only for the solution approximation but also for the computation of the integrals arising from the weak variational form. Unfortunately, despite its high numerical accuracy along with some recent developments [Atluri, Liu and Han (2006a); Atluri, Liu and Han (2006b)], MLPG appears to suffer from two major drawbacks: 1) the numerical computation of the integrals arising from the local weak form can be very expensive because of the non-polynomial form of the MLS shape functions and the possibly irregular support of the test functions [Mazzia, Ferronato, Pini and Gambolati (2007); Mazzia and Pini (2010)]; 2) the Dirichlet boundary conditions cannot be prescribed in a strong way because the MLS shape functions do not possess the Kronecker-delta property [Fernandez-Mendez and Huerta (2004)]. Therefore, coupling FE and meshfree methods seems a reasonable trade-off to take advantage of both approaches.

Several authors have proposed different alternatives to blend FE and meshfree

methods. These techniques are developed for two main purposes: 1) coupling FE-discretized with meshless regions, and 2) enriching the FE approximation space with shape functions associated to meshless particles. The first approach is generally preferred in composite simulations where three regions can be identified, one discretized by FE, one by meshless particles, and one is a transition zone. Examples of such a strategy can be found in [Belytschko, Organ and Krongauz (1995)] and [Hegen (1996)]. In the second approach a relatively coarse FE mesh of the integration domain is enriched by adding meshless particles wherever an improvement of the solution accuracy is needed. One of the earliest examples of an enriched approach can be found in [Liu, Uras and Chen (1997)] while a more general formulation is developed in [Huerta and Fernandez-Mendez (2000)].

The present paper describes a FE enrichment by MLPG. The main purpose of the proposed approach is threefold. First, locally improving a FE solution with MLPG nodes avoids the need for progressive grid refinements and re-meshing processes, especially in transient problems where the potentially intensive re-meshing effort can be replaced by an inexpensive motion of meshless particles. Second, using few MLPG points into a FE-discretized domain adds a limited computational burden. Third, the Dirichlet boundary can be efficiently discretized by FE only, thus allowing for the prescription of the essential conditions in a strong way. The paper is organized as follows. After a brief MLPG overview, the enriched approach is described for a linear differential problem along with its numerical implementation. The method is derived in detail for a transient Poisson problem and validated against analytical solutions. In particular, a convergence analysis is perfomed as compared to traditional FE. Finally, some remarks on the preliminary results and the on-going work close the paper.

2 Finite Element enrichment by MLPG

2.1 MLPG overview

MLPG is a meshless variational method based on the MLS approximation scheme. Consider a bounded domain Ω and let $u^h(\mathbf{x})$ be the unknown trial approximant of $u(\mathbf{x})$ in Ω. The basic idea is to find u^h at a given point $\mathbf{x}$ using a polynomial least-squares fit of u in a neighbourhood of $\mathbf{x}$. Choosing $\mathbf{x} \in \Omega$ and $\mathbf{z}$ near $\mathbf{x}$, $u^h(\mathbf{z},\mathbf{x})$ has the polynomial expression:

$$u^h(\mathbf{z},\mathbf{x}) = \sum_{i=1}^{m} p_i(\mathbf{z}) a_i(\mathbf{x}) = \mathbf{p}^T(\mathbf{z})\mathbf{a}(\mathbf{x}) \tag{1}$$

where $\mathbf{p}^T(\mathbf{z}) = [p_1(\mathbf{z}), p_2(\mathbf{z}), \ldots, p_m(\mathbf{z})]$ is the vector of the complete monomial basis of size m, and $\mathbf{a}(\mathbf{x}) = [a_1(\mathbf{x}), a_2(\mathbf{x}), \ldots, a_m(\mathbf{x})]^T$ is the vector of the unknown

coefficients $a_j(\mathbf{x})$, $j = 1, \ldots, m$. The coefficient vector $\mathbf{a}(\mathbf{x})$ is obtained by a local least-square fit that minimizes the discrete functional $J(\mathbf{a})$:

$$J(\mathbf{a}) = \sum_{\mathbf{x}_i \in \Omega_x} w_i(\mathbf{x})[\mathbf{p}^T(\mathbf{x}_i)\mathbf{a}(\mathbf{x}) - \hat{u}_i]^2 \tag{2}$$

where w_i is the weight function associated with node $\mathbf{x}_i$, $\hat{u}_i$ a fictitious nodal value and Ω_x is the domain of definition of $\mathbf{x}$, which covers all the nodes whose weight function does not vanish at $\mathbf{x}$. Defining the Gram matrix $M(\mathbf{x})$ as:

$$M(\mathbf{x}) = \sum_{\mathbf{x}_i \in \Omega_x} w_i(\mathbf{x})\mathbf{p}(\mathbf{x}_i)\mathbf{p}^T(\mathbf{x_i}) \tag{3}$$

minimization of Eq. 2 with respect to $\mathbf{a}$ yields:

$$u^h(\mathbf{z}, \mathbf{x}) = \mathbf{p}^T(\mathbf{z})M^{-1}(\mathbf{x}) \sum_{\mathbf{x}_i \in \Omega_x} w_i(\mathbf{x})\mathbf{p}(\mathbf{x}_i)\hat{u}_i \tag{4}$$

which particularized at $\mathbf{z} = \mathbf{x}$ leads to the discrete MLS approximation:

$$u^h(\mathbf{x}) = \sum_{\mathbf{x}_i \in \Omega_x} w_i(\mathbf{x})\mathbf{p}^T(\mathbf{x})M^{-1}(\mathbf{x})\mathbf{p}(\mathbf{x}_i)\hat{u}_i = \sum_{\mathbf{x}_i \in \Omega_x} \Phi_i(\mathbf{x})\hat{u}_i \tag{5}$$

The function $\Phi_i(\mathbf{x})$ is the MLS shape function associated to point $\mathbf{x}_i$. Note that $u^h(\mathbf{x}_i) \neq \hat{u}_i$ because $\Phi_i(\mathbf{x})$ is not interpolant. A necessary condition for the computation of $\Phi_i(\mathbf{x})$ is the non-singularity of $M(\mathbf{x})$. This is ensured if there are enough particles $\mathbf{x}_i$ in the neighbourhood of $\mathbf{x}$ avoiding degenerate patterns, e.g. aligned points. For details see for instance [Liu, Li and Belytschko (1997)].

The trial approximant u^h is computed writing a variational formulation of the general differential problem $Au(\mathbf{x}) = f(\mathbf{x})$:

$$\int_{\Omega_s} \Big(Au^h(\mathbf{x}) - f(\mathbf{x}) \Big) v_i \, \mathrm{d}\Omega - \alpha \int_{\Gamma_{su}} \Big(u^h(\mathbf{x}) - \overline{u}(\mathbf{x}) \Big) v_i \, \mathrm{d}\Gamma = 0 \quad i = 1, \ldots, n \tag{6}$$

where Ω_s is the support of the test functions v_i and n is the number of particles. Ω_s is also called domain of influence of node $\mathbf{x}_i$ and is usually a circle centered at $\mathbf{x}_i$. Dirichlet conditions $\overline{u}$ over Γ_{su} are prescribed in a weak way using the penalty α. Introducing Eq. 5 into Eq. 6 yields the $n \times n$ linear system:

$$K_M \hat{\mathbf{u}} = \mathbf{f} \tag{7}$$

which allows for computing the vector of fictitious nodal values $\hat{\mathbf{u}}$. The matrix K_M collects the numerical integrals computed with Eq. 6 and is the MLPG stiffness matrix. Back-substitution of the $\hat{\mathbf{u}}$ components into Eq. 5 provides the desired meshless solution.

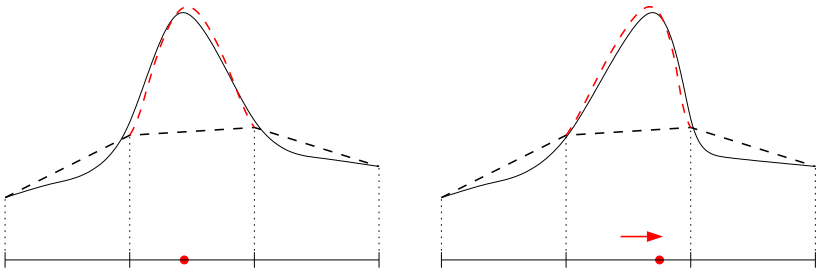

Figure 1: Example of enriched solution (left) and its evolution in time with no re-meshing (right).

2.2 Enrichment of FE approximation space

Let us briefly introduce the basic idea of the proposed enrichment with the elementary 1-D example of Fig. 1. We want to approximate the function plotted with a solid black line. Using a coarse discretization by linear FE we are likely to obtain the dashed black profile, with possible large errors especially far from the element nodes. A more accurate result can be attained superimposing on the FE trial function the MLS approximation associated with some meshless points, as is shown in Fig. 1. The possible evolution in time can be followed by moving the meshless points only instead of re-meshing the domain.

From a mathematical viewpoint, the trial function u^h can be described as the superimposition of FE and MLS approximations:

$$u^h(\mathbf{x}) = \sum_{j=1}^{n_{FE}} \xi_j(\mathbf{x})\tilde{u}_j + \sum_{i=1}^{n_{ML}} \Phi_i(\mathbf{x})\hat{u}_i \tag{8}$$

where n_{FE} and n_{ML} is the number of FE nodes and meshless points, respectively, and $\xi_j(\mathbf{x})$ is the FE shape function associated with node j. As generally $\Phi_i(\mathbf{x}_j) \neq 0$, the coefficient $\tilde{u}_j$ is no longer the numerical approximation of $u(\mathbf{x}_j)$. Using Eq. 8 we seek an approximation of u in the functional space generated by both FE and MLS shape functions, i.e. the FE approximation space is enriched by the MLS functions. The non-polynomial form of $\Phi_i(\mathbf{x})$ and the shape of its support ensure that the set of functions Φ_i and ξ_j is linearly independent.

The coefficients $\tilde{u}_j$ and $\hat{u}_i$ can be computed writing a variational form of the differential problem $Au(\mathbf{x}) = f(\mathbf{x})$:

$$\begin{cases} \displaystyle\int_\Omega \Big(Au^h(\mathbf{x}) - f(\mathbf{x})\Big)\,\xi_j(\mathbf{x})\,\mathrm{d}\Omega = 0 & j = 1,\ldots,n_{FE} \\ \displaystyle\int_\Omega \Big(Au^h(\mathbf{x}) - f(\mathbf{x})\Big)\,v_i(\mathbf{x})\,\mathrm{d}\Omega = 0 & i = 1,\ldots,n_{ML} \end{cases} \tag{9}$$

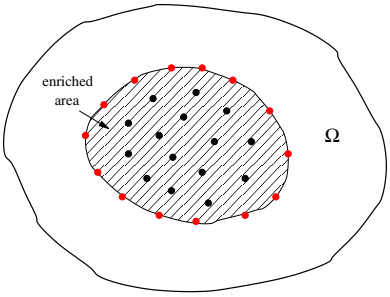

Figure 2: MLPG points where fictitious zero Dirichlet conditions are prescribed are located on the boundary of the inner enriched region.

where as test functions we use the FE basis ξ_j, $j = 1,\ldots,n_{FE}$, i.e. a Galerkin approach, and n_{ML} additional independent functions v_i. Following the so-called MLPG1 approach [Atluri (2004)], we set $v_i(\mathbf{x}) = w_i(\mathbf{x})$. Other choices for v_i are of course possible and can be the object of further investigations. Assuming the differential operator A to be linear and recalling Eq. 8, Eq. 9 reads:

$$\begin{cases} \sum_{k=1}^{n_{FE}} \left[\int_\Omega \xi_j A \xi_k \mathrm{d}\Omega \right] \tilde{u}_k + \sum_{k=1}^{n_{ML}} \left[\int_\Omega \xi_j A \Phi_k \mathrm{d}\Omega \right] \hat{u}_k = \int_\Omega \xi_j f \ \mathrm{d}\Omega \quad j = 1, n_{FE} \\ \sum_{k=1}^{n_{FE}} \left[\int_\Omega v_i A \xi_k \mathrm{d}\Omega \right] \tilde{u}_k + \sum_{k=1}^{n_{ML}} \left[\int_\Omega v_i A \Phi_k \mathrm{d}\Omega \right] \hat{u}_k = \int_\Omega v_i f \ \mathrm{d}\Omega \quad i = 1, n_{ML} \end{cases} \tag{10}$$

that in matrix form becomes:

$$\begin{cases} K_F \tilde{\mathbf{u}} + K_{FM} \hat{\mathbf{u}} = \mathbf{b}_F \\ K_{MF} \tilde{\mathbf{u}} + K_M \hat{\mathbf{u}} = \mathbf{b}_M \end{cases} \quad \Rightarrow \quad K\mathbf{u} = \mathbf{b} \tag{11}$$

where K_F and K_M are the FE and MLPG stiffness matrix, respectively, K_{FM} and K_{MF} are coupling blocks, and $\mathbf{b}_F$ and $\mathbf{b}_M$ are the FE and MLPG forcing vectors, respectively. Note that $K_{FM} \neq K_{MF}^T$ and $K_M \neq K_M^T$, hence K is unsymmetric. Note that the integrals in Eq. (10) can be restricted to a local domain where both the test and trial functions are non-zero. Such local domains are the union of FEs sharing nodes j and k to compute the K_F entries, the domain of influence Ω_s of the test function v_i for K_M, the union of FEs sharing node j with the domain of definition of the MLS shape function Φ_k for K_{FM}, and finally the union of the domain of influence Ω_s of v_i with the FEs sharing node k in K_{MF}.

Eq. 11 must be solved prescribing the essential boundary conditions over Γ_{su}, so that K is guaranteed to be non-singular. Suppose Γ_{su} to be discretized by FE only, i.e. $\Phi_i(\mathbf{x}) = 0$ for every i at any $\mathbf{x} \in \Gamma_{su}$. Hence, Dirichlet conditions can be imposed

in a strong way setting the diagonal entries of K corresponding to the FE nodes over Γ_{su} to 1 and all the off-diagonal entries to 0, with the first n_{FE} rows in Eq. 11 now independent. The last n_{ML} rows, however, can still be dependent. To avoid such an occurrence, we can constrain the MLS approximation to coincide with the FE solution at the boundary of the enriched region. This can be done by imposing that $\hat{u}_i = 0$ for the MLPG points located on such internal boundary (Fig. 2 for a 2-D domain), i.e. fictitious zero Dirichlet conditions are prescribed over a subset of MLPG points. Hence, inside the enriched region the solution is a superimposition of FE and MLPG, outside the MLPG contribution is null and a compatibility condition is imposed at the interface between the two regions.

The biggest effort for computing matrix K of Eq. 11 stems from the calculation of the coupling blocks K_{FM} and K_{MF} because numerical integrals over intersections and unions of circles, circular sectors and polygons must be performed after the identification of the connections between FE nodes and MLPG points. A simple approximation can be done just neglecting one of the two blocks, or both. The quality of such an approximation depends on the size of the neglected terms, i.e. on the size of the supports of Φ_i and v_i. For example, neglecting K_{FM} the solution to Eq. 11 can be obtained by a two-step algorithm:

$$K_F \tilde{\mathbf{u}} = \mathbf{b}_F \tag{12}$$

$$K_M \hat{\mathbf{u}} = \mathbf{b}_M - K_{MF} \tilde{\mathbf{u}} \tag{13}$$

where Eq. 12 is often symmetric and positive definite and the unsymmetric Eq. 13 is typically much less difficult than Eq. 11 as $n_{ML} \ll n_{FE}$. This simplified and much cheaper approach gives rise to an uncoupled FE-MLPG enrichment.

3 Application to a transient Poisson problem

The enriched approach has been tested in 2-D transient Poisson problems with a diffusion coefficient D:

$$D\nabla^2 u(\mathbf{x},t) = \dot{u}(\mathbf{x},t) + f(\mathbf{x},t) \tag{14}$$

using time-independent FE and MLS shape functions. A weak form for the variational Eq. 9 can be conveniently developed incorporating naturally the Neumann boundary conditions into the forcing vectors. The numerical formulation reads:

$$\begin{cases} H_F \tilde{\mathbf{u}} + H_{FM} \hat{\mathbf{u}} + P_F \dot{\tilde{\mathbf{u}}} + P_{FM} \dot{\hat{\mathbf{u}}} = \mathbf{q}_F \\ H_{MF} \tilde{\mathbf{u}} + H_M \hat{\mathbf{u}} + P_{MF} \dot{\tilde{\mathbf{u}}} + P_M \dot{\hat{\mathbf{u}}} = \mathbf{q}_M \end{cases} \tag{15}$$

where H_F, H_M, P_F and P_M are the classical FE and MLPG stiffness and capacity matrices, respectively:

$$[H_F]_{ij} = \int_\Omega D\nabla\xi_i\nabla\xi_j \,\mathrm{d}\Omega, \quad i,j=1,\ldots,n_{FE}, \tag{16}$$

$$[H_M]_{ij} = \int_\Omega D\nabla\Phi_i\nabla v_j \,\mathrm{d}\Omega, \quad i,j=1,\ldots,n_{ML}, \tag{17}$$

$$[P_F]_{ij} = \int_\Omega \xi_i\xi_j \,\mathrm{d}\Omega, \quad i,j=1,\ldots,n_{FE}, \tag{18}$$

$$[P_M]_{ij} = \int_\Omega \Phi_i v_j \,\mathrm{d}\Omega, \quad i,j=1,\ldots,n_{ML}, \tag{19}$$

H_{FM}, H_{MF}, P_{FM} and P_{MF} are the rectangular coupling blocks:

$$[H_{FM}]_{ij} = \int_\Omega D\nabla\xi_i\nabla\Phi_j \,\mathrm{d}\Omega, \quad i=1,\ldots,n_{FE}, \quad j=1,\ldots,n_{ML}, \tag{20}$$

$$[H_{MF}]_{ij} = \int_\Omega D\nabla v_i\nabla\xi_j \,\mathrm{d}\Omega, \quad i=1,\ldots,n_{ML}, \quad j=1,\ldots,n_{FE}, \tag{21}$$

$$[P_{FM}]_{ij} = \int_\Omega \xi_i\Phi_j \,\mathrm{d}\Omega, \quad i=1,\ldots,n_{FE}, \quad j=1,\ldots,n_{ML}, \tag{22}$$

$$[P_{MF}]_{ij} = \int_\Omega v_i\xi_j \,\mathrm{d}\Omega, \quad i=1,\ldots,n_{ML}, \quad j=1,\ldots,n_{FE}, \tag{23}$$

and $\mathbf{q}_F$ and $\mathbf{q}_M$ are the forcing vectors:

$$[\mathbf{q}_F]_i = \int_\Gamma \xi_i\nabla u\cdot\mathbf{n} \,\mathrm{d}\Gamma - \int_\Omega \xi_i f \,\mathrm{d}\Omega, \quad i=1,\ldots,n_{FE}, \tag{24}$$

$$[\mathbf{q}_M]_i = \int_\Gamma v_i\nabla u\cdot\mathbf{n} \,\mathrm{d}\Gamma - \int_\Omega v_i f \,\mathrm{d}\Omega, \quad i=1,\ldots,n_{ML}, \tag{25}$$

with Γ the Neumann boundary and $\mathbf{n}$ its outer normal.

Eq. 15 is a discrete system of linear ordinary differential equations in time which can be integrated by a finite difference marching scheme. Writing Eq. 15 in the classical compact form $H\mathbf{u}+P\dot{\mathbf{u}}=\mathbf{q}$ with:

$$H=\begin{bmatrix} H_F & H_{FM} \\ H_{MF} & H_M \end{bmatrix}, \quad P=\begin{bmatrix} P_F & P_{FM} \\ P_{MF} & P_M \end{bmatrix}, \quad \mathbf{u}=\begin{Bmatrix} \tilde{\mathbf{u}} \\ \hat{\mathbf{u}} \end{Bmatrix}, \quad \mathbf{q}=\begin{Bmatrix} \mathbf{q}_F \\ \mathbf{q}_M \end{Bmatrix} \tag{26}$$

the solution at time $t+\Delta t$ is obtained by solving:

$$\left(\theta H+\frac{P}{\Delta t}\right)\mathbf{u}^{(t+\Delta t)} = \left[\frac{P}{\Delta t}-(1-\theta)H\right]\mathbf{u}^{(t)}+\theta\mathbf{q}^{(t+\Delta t)}+(1-\theta)\mathbf{q}^{(t)} \tag{27}$$

where θ is a user-specified parameter between 0 and 1. Eq. 27 is repeatedly solved starting from the initial condition until steady state, if any.

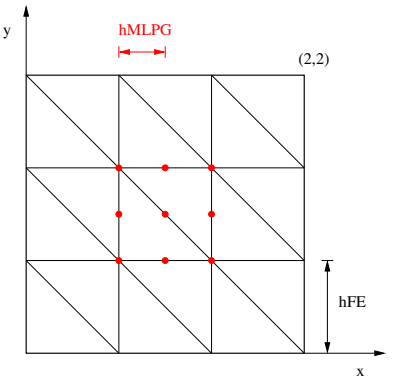

Figure 3: Domain and enriched region for the transient Poisson test problems.

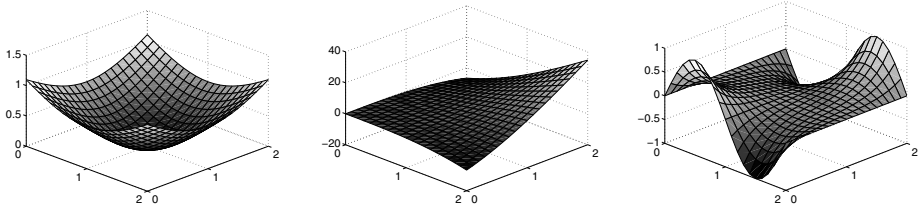

Figure 4: Analytical solution for the tests: "steady 1" (left), "steady 2" (middle), "steady 3" (right).

3.1 Numerical results

Eq. 14 is numerically solved for different choices of the forcing function $f(\mathbf{x},t)$, the diffusion coefficient D and analytical solutions $u(\mathbf{x},t)$ over the $[0,2]\times[0,2]$ square domain with Dirichlet conditions prescribed at the boundary. The domain is discretized into linear triangular FE and enriched by MLPG points in the central $[2/3,4/3]\times[2/3,4/3]$ square region (Fig. 3). Accuracy of the solution at the instant t is checked through the relative error $\varepsilon(t)$:

$$\varepsilon(t)=\frac{\sqrt{\sum_{j=1}^{n_{FE}}\left[u\left(\mathbf{x}_j,t\right)-u^h\left(\mathbf{x}_j,t\right)\right]^2+\sum_{i=1}^{n_{ML}}\left[u\left(\mathbf{x}_i,t\right)-u^h\left(\mathbf{x}_i,t\right)\right]^2}}{\sqrt{\sum_{j=1}^{n_{FE}}u^2\left(\mathbf{x}_j,t\right)+\sum_{i=1}^{n_{ML}}u^2\left(\mathbf{x}_i,t\right)}} \tag{28}$$

Both steady state and transient problems are investigated.

3.1.1 Steady state problem

Three analytical test cases are considered with $D=1$:

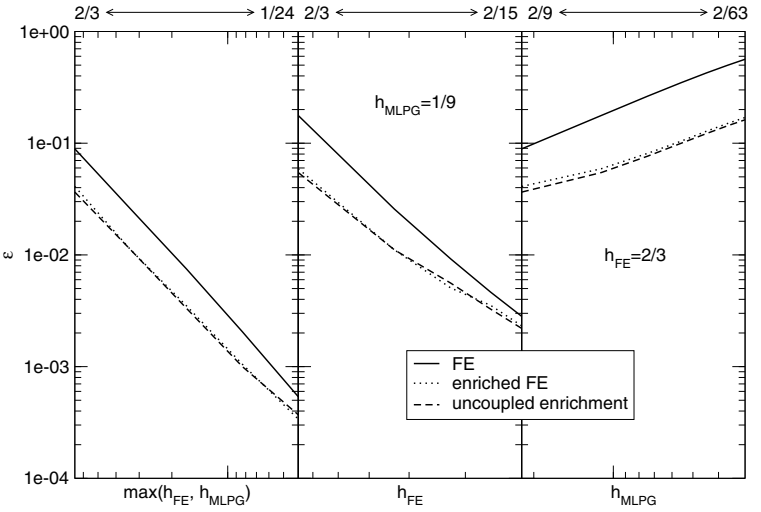

Figure 5: Convergence analysis for the "steady 1" test case. On the x-axis h_{FE} and h_{MLPG} are reported in descending order.

- Steady 1: $u(x,y) = \log[1+(x-1)^2+(y-1)^2]$;
- Steady 2: $u(x,y) = -\frac{5}{6}(x^3+y^3)+3x^2y+3xy^2$;
- Steady 3: $u(x,y) = [\cosh(\pi y) - \operatorname{cotanh}(\pi)\sinh(\pi y)]\sin(\pi x)$.

A sketch of the function plots is shown in Fig. 4. Notice the different scale on the vertical axis. The convergence of the enriched approach is investigated vs. the average element size h_{FE} and distance between meshless points h_{MLPG} (see Fig. 3). Fig. 5 shows in a double log-log plot the variation of ε (Eq. 28) as h_{FE} and h_{MLPG} are progressively decreased for the "steady 1" test case. Notice that the values on the x-axis of Fig. 5 are reported in descending order. The leftmost diagram of Fig. 5 provides ε as both h_{FE} and h_{MLPG} decrease, i.e. the FE grid is progressively refined and the number of meshless points increased. Both the coupled and the uncoupled enriched methods converge linearly with the same rate as FE alone but with a smaller error, thus being effective in improving the solution accuracy. The middle diagram of Fig. 5 shows the ε variation refining the FE grid only. The convergence of the enriched methods slightly deteriorates as h_{FE} decreases. This is because the size of the FE approximation space progressively increases while the MLS one does not, so the enrichment still works though at a lesser extent. Finally, the rightmost diagram shows the ε variation increasing the number of meshless points over a fixed (coarse) grid. The FE method alone does not converge as the

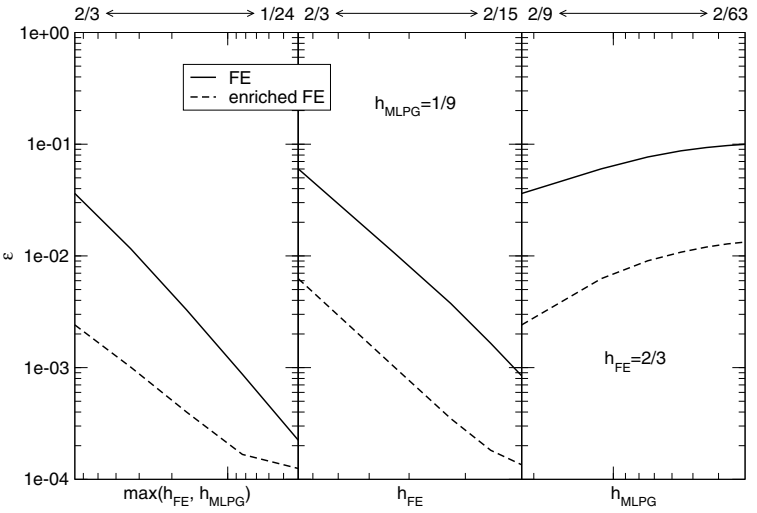

Figure 6: The same as Fig. 5 for the "steady 2" test case.

size of the space generated by ξ_j is not increasing. The enrichment always provides more accurate results with smaller ε, but convergence is not achieved. This is not because of MLPG, rather the fictitious zero Dirichlet conditions prescribed on a few meshless points which constrain the MLS approximation to coincide with the FE solution at the boundary of the enriched region. As FE do not converge to the analytical solution, the enriched method is enforced to follow. In other words, the MLPG enrichment accelerates the convergence to the FE approximation obtained with a given grid, which is obviously not the "right" solution. Note also that coupled and uncoupled enrichments provide practically the same results. This is not a general conclusion, but wherever possible the uncoupled approach is to be preferred because of its smaller computational cost.

Fig. 6 and Fig. 7 provide the same result as Fig. 5 for the "steady 2" and "steady 3" test cases, respectively. In these problems only the most accurate enrichment between the coupled and the uncoupled one is shown. The same conclusions as for the "steady 1" test case can be argued, with however, significant differences in the size of the actual improvement allowed for by the enrichment. The reason becomes apparent recalling Fig. 4. The "steady 2" function displays a very irregular behavior in the enriched region, while the "steady 3" function is quite flat. Therefore, the proposed enrichment appears to be very effective wherever steep variations of u are expected.

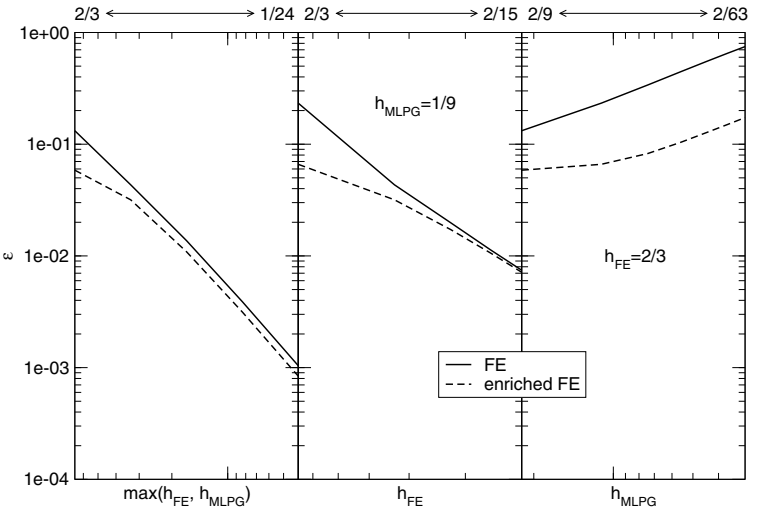

Figure 7: The same as Fig. 5 for the "steady 3" test case.

3.1.2 Transient solution

Two analytical test cases are considered with $D = 10^{-5}$:

- Trans 1: $u(x,y,t) = 1 + e^{-\pi^2 Dt}\sin(\pi x)\sin(\pi y)$;
- Trans 2: $u(x,y,t) = 1 + \text{atan}(Dt)(x^2 - x)(y^2 - y)$.

A sketch of the function plots is shown in Fig. 8 and Fig. 9. Note that in the transient simulations the domain has been scaled to the $[0,1]\times[0,1]$ square with the meshless points regularly distributed in the central $[1/4,3/4]\times[1/4,3/4]$ square. A constant Δt is selected for each simulation such that $h_{FE}/D\Delta t = 100$, while θ in Eq. 27 is set to 1, i.e. a backward difference scheme is used.

Fig. 10 and Fig. 11 provide ε vs. h_{FE} and h_{MLPG} for the "trans 1" and "trans 2" test case, respectively, at $t_0 = 250$ and $t_{inf} = 50000$. As the "trans 1" analytical solution evolves towards a constant steady state (Fig. 8), the improvement guaranteed by the enriched technique should decrease as time proceeds. This is due to the fact that a constant solution can be exactly obtained in the space of the FE basis functions. Therefore, the enrichment provided by the MLS shape functions is somewhat useless with the fictitious values $\hat{\mathbf{u}}$ approaching zero. This is shown in the leftmost and middle diagrams of Fig. 10 with the convergence rate exhibited by the enriched technique stagnating because of the truncation error of the marching scheme. Similarly to the steady state cases, convergence is not ensured when h_{MLPG}

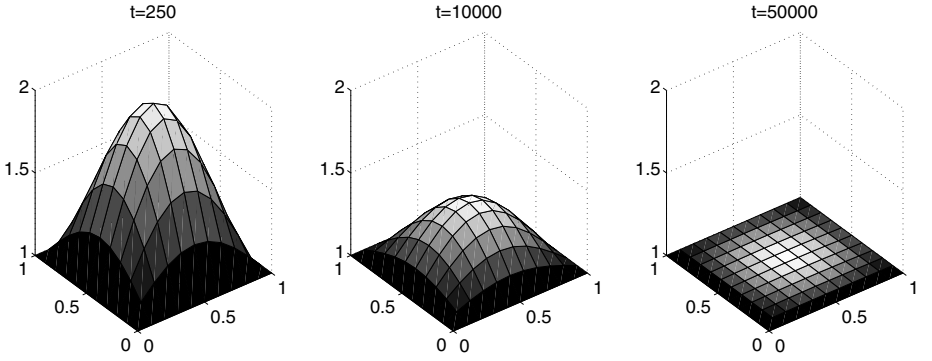

Figure 8: Analytical solution in time for the "trans 1" test case.

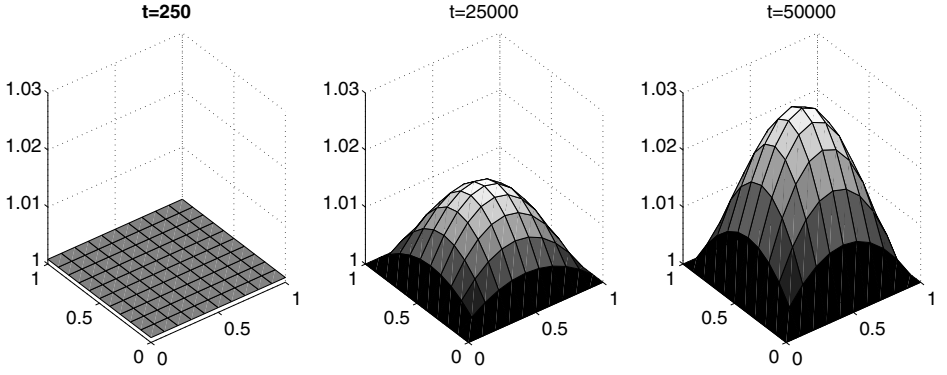

Figure 9: Analytical solution in time for the "trans 2" test case.

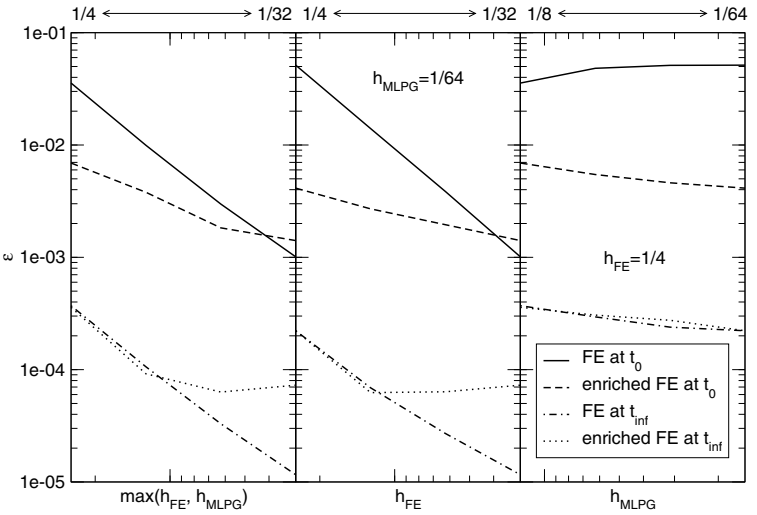

Figure 10: Convergence analysis for the "trans 1" test case at different times.

only is decreased, even though the enriched technique exhibits a slight numerical improvement. The "trans 2" test case in Fig. 11 exhibits an inverse behavior, with the enriched technique yielding better results approaching the steady state because the analytical solution evolves in time differently from the "trans 1" problem (see Fig. 9).

A summary of the results is finally provided in Fig. 12 showing the ratio between ε computed using FE only and the enriched method. Generally, this ratio decreases with h_{FE} and h_{MLPG}, i.e. the effectiveness of the enrichment diminuishes as the grid and the meshless point distribution are refined. With steep and irregular solutions, however, the enriched technique is up to 15 times more accurate than FE alone using a small number of MLPG points, thus allowing for a significant improvement of the approximation accuracy and avoiding the need of a domain re-meshing.

4 Conclusions

A simple strategy for blending FE and meshless methods is proposed with the aim at exploiting the attractive properties of each approximation technique. FE computations with no re-meshing can be very efficient and allow for a straightforward way of prescribing the Dirichlet essential conditions. Meshless methods based on the MLS scheme can be very accurate even using few points which can be easily moved throughout the domain to follow the solution variation in time. The FE enrichment by MLPG is a variational technique where the trial approximant is ob-

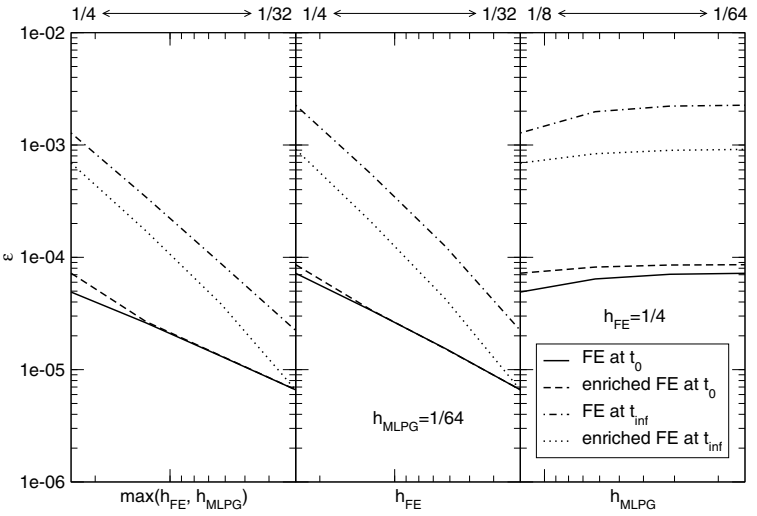

Figure 11: The same as Fig. 10 for the "trans 2" test case.

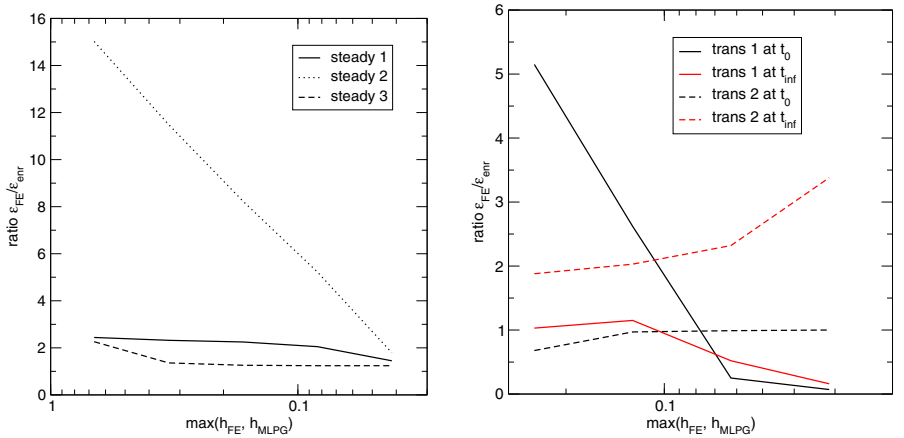

Figure 12: Ratio between ε computed with FE only and with the enrichment: steady state (left) and transient (right) test problems.

tained by a linear combination of FE and MLS shape functions. As test functions both the FE shape functions and the MLS local weights are used.

The proposed enrichment has been tested in a number of steady state and transient Poisson problems. The accuracy of the trial solution is always better than using FE only by up to a factor 15. The most significant improvements are obtained

describing irregular functions with a coarse mesh and a small number of meshless points. Moreover, the enriched method converges to the analytical solution roughly with the same rate as FE when both the underlying grid and the meshless point distribution are regularly refined.

Some work is currently underway to improve the present formulation. A modified formulation is being developed to ensure convergence of the enriched solution when the number of MLPG points only is increased. Experiments are on-going on different quadrature rules in order to improve the accuracy and the computational efficiency of the numerical integrals arising in the enriched formulation. These experiments will be performed in problems larger than those discussed in the present paper so as to allow for a significant comparison in terms of CPU time of a standard FE method with the enriched FE-MLPG technique to gain the same numerical accuracy. Finally, additional tests on more challenging problems, such as the mechanics of bodies with large domain deformation, including object penetrations into a structure, are going to be investigated using the FE-MLPG enriched approach.

Acknowledgement: This work has been partially funded by the Italian MIUR project (PRIN) "Advanced numerical methods and models for enviromental fluid-dynamics and geomechanics".

References

Atluri, S. N. (2004): *The Meshless Local Petrov-Galerkin (MLPG) Method*. Tech. Science Press.

Atluri, S. N.; Zhu, T. (1998): A new meshless local Petrov-Galerkin (MLPG) approach in computational mechanics. *Computational Mechanics*, vol. 22, pp. 117–127.

Atluri, S. N.; Liu, H. T.; Han, Z. D. (2006a): Meshless Local Petrov-Galerkin (MLPG) mixed collocation method for elasticity problems. *CMES: Computer Modeling in Engineering & Sciences*, vol. 14, no. 3, pp. 141–152.

Atluri, S. N.; Liu, H. T.; Han, Z. D. (2006b): Meshless Local Petrov-Galerkin (MLPG) mixed finite difference method for solid mechanics. *CMES: Computer Modeling in Engineering & Sciences*, vol. 15, no. 1, pp. 1–16.

Avila, R.; Atluri, S. N. (2010): Numerical solution of non-steady flows, around surfaces in spatially and temporally arbitrary motion, by using the MLPG method. *CMES: Computer Modeling in Engineering & Sciences*, vol. 54, no. 1, pp. 15–64.

Belytschko, T.; Lu, Y. Y.; Gu, L. (1994): Element-free Galerkin methods. *International Journal for Numerical Methods in Engineering*, vol. 37, pp. 229–256.

Belytschko, T.; Organ, D.; Krongauz, Y. (1995): A coupled finite element–element-free Galerkin method. *Computational Mechanics*, vol. 17, pp. 186–195.

Bergamaschi, L.; Martinez, A.; Pini, G. (2009): An efficient parallel MLPG method for poroelastic models. *CMES: Computer Modeling in Engineering & Sciences*, vol. 49, no. 3, pp. 191–216.

Ching, H. K.; Chen, J. K. (2006): Thermomechanical analysis of functionally graded composites under laser heating by the MLPG method. *CMES: Computer Modeling in Engineering & Sciences*, vol. 13, no. 3, pp. 199–217.

Deeks, A. J.; Augarde, C. E. (2007): A hybrid meshless local Petrov-Galerkin method for unbounded domains. *Computer Methods in Applied Mechanics and Engineering*, vol. 196, pp. 843–852.

Fernandez-Mendez, S.; Bonet, J.; Huerta, A. (2005): Continuous blending of SPH with finite elements. *Computers & Structures*, vol. 83, pp. 1448–1458.

Fernandez-Mendez, S.; Huerta, A. (2004): Imposing essential boundary conditions in meshfree methods. *Computer Methods in Applied Mechanics and Engineering*, vol. 193, pp. 1257–1275.

Ferronato, M.; Mazzia, A.; Pini, G.; Gambolati, G. (2007): A meshless method for axi-symmetric poroelastic simulations: numerical study. *International Journal for Numerical Methods in Engineering*, vol. 70, pp. 1346–1375.

Gao, L.; Liu, K.; Liu, Y. (2006): Applications of MLPG method in dynamic fracture problems. *CMES: Computer Modeling in Engineering & Sciences*, vol. 12, no. 3, pp. 181–195.

Han, Z. D.; Rajendran, A. M.; Atluri, S. N. (2005): Meshless Local Petrov–Galerkin (MLPG) approaches for solving nonlinear problems with large deformations and rotations. *CMES: Computer Modeling in Engineering & Sciences*, vol. 10, no. 1, pp. 1–12.

Han, Z. D.; Liu, H. T.; Rajendran, A. M.; Atluri, S. N. (2006): The applications of Meshless Local Petrov-Galerkin (MLPG) approaches in high-speed impact, penetration and perforation problems. *CMES: Computer Modeling in Engineering & Sciences*, vol. 14, no. 2, pp. 119–128.

Heaney, C.; Augarde, C.; Deeks, A. (2010): Modelling elasto-plasticity using the Hybrid MLPG method. *CMES: Computer Modeling in Engineering & Sciences*, vol. 56, no. 2, pp. 153–176.

Hegen, D. (1996): Element free Galerkin methods in combination with finite element approaches. *Computer Methods in Applied Mechanics and Engineering*, vol. 135, pp. 143–166.

Huerta, A.; Fernandez-Mendez, S. (2000): Enrichment and coupling of the finite element and meshless methods. *International Journal for Nuemrical Methods in Engineering*, vol. 48, pp. 1615–1636.

Johnson, J. N.; Owen, J. M. (2007): A Meshless Local Petrov-Galerkin method for magnetic diffusion in non-magnetic conductors. *CMES: Computer Modeling in Engineering & Sciences*, vol. 22, no. 3, pp. 165–188.

Liu, W. K.; Jun, S.; Zhang, Y. F. (1995): Reproducing kernel particle methods. *International Journal for Numerical Methods in Fluids*, vol. 20, pp. 1081–1106.

Liu, W. K.; Li, S.; Belytschko, T. (1997): Moving least square reproducing kernel particle methods. Part I: Methodology and convergence. *Computer Methods in Applied Mechanics and Engineering*, vol. 143, pp. 113–154.

Liu, W. K.; Uras, R. A.; Chen, Y. (1997): Enrichment of the finite element method with the reproducing kernel particle. *Journal of Applied Mechanics*, vol. 64, pp. 861–870.

Liu, F.; Borja, R. I. (2008): A contact algorithm for frictional crack propagation with the extended finite element method. *International Journal for Numerical Mehods in Engineering*, vol. 76, pp. 1489–1512.

Mazzia, A.; Ferronato, M.; Pini, G.; Gambolati, G. (2007): A comparison of numerical integration rules for the meshless local Petrov-Galerkin method. *Numerical Algorithms*, vol. 45, pp. 61–74.

Mazzia, A.; Pini, G. (2010): Product Gauss quadrature rules vs. cubature rules in the meshless local Petrov-Galerkin method. *Journal of Complexity*, vol. 26, pp. 82–101.

Randles, P. W.; Libersky, L. D. (1996): Smoothed particle hydrodynamics: some recent improvements and applications. *Computer Methods in Applied Mechanics and Engineering*, vol. 139, pp. 375–408.

Randles, P. W.; Libersky, L. D. (2000): Normalised SPH with stress points. *International Journal for Numerical Mehods in Engineering*, vol. 48, pp. 1445–1462.

Sladek, J.; Sladek, V.; Zhang, C.; Tan, C. L. (2006): Meshless Local Petrov-Galerkin method for linear coupled thermoelastic analysis. *CMES: Computer Modeling in Engineering & Sciences*, vol. 16, no. 1, pp. 57–68.

Sladek, J.; Sladek, V.; Zhang, Ch.; Solek, P.; Starek, L. (2007): Fracture analyses in continuously nonhomogeneous piezoelectric solids by the MLPG. *CMES: Computer Modeling in Engineering & Sciences*, vol. 19, no. 3, pp. 247–262.

Wang, D.; Chen, J. S.; Sun, L. (2003): Homogenization of magnetostrictive particle-filled elastomers using an interface-enriched reproducing kernel particle method. *Finite Elements in Analysis and Design*, vol. 39, pp. 765–782.

Wells, G. N.; Borst, R.; Sluys, L. J. (2002): A consistent geometrically non-linear approach for delamination. *International Journal for Numerical Mehods in Engineering*, vol. 54, pp. 1333–1355.

Wu, X. H.; Shen, S. P.; Tao, W. Q. (2007): Meshless Local Petrov-Galerkin collocation method for two-dimensional heat conduction problems. *CMES: Computer Modeling in Engineering & Sciences*, vol. 22, no. 1, pp. 65–76.